Published in final edited form as:
*J Magn Reson*. 2009 June ; 198(2): 188–196. doi:10.1016/j.jmr.2009.02.005.

# Multi-components of T2 Relaxation in *ex vivo* Cartilage and Tendon

**ShaoKuan Zheng, PhD** and **Yang Xia, PhD***
Department of Physics and Center for Biomedical Research, Oakland University, Rochester, MI 48309

## Abstract

The multi-components of $T_2$ relaxation in cartilage and tendon were investigated by microscopic MRI (μMRI) at 13μm and 26μm transverse resolutions. Two imaging protocols were used to quantify $T_2$ relaxation in the specimens, a 5-point sampling and a 60-point sampling. Both multi-exponential and non-negative-least-square (NNLS) fitting methods were used to analyze the μMRI signal. When the imaging voxel size was $6.76\times10^{-4}$ $mm^3$ and within the limit of practical signal-to-noise ratio (SNR) in microscopic imaging experiments, we found that (1) canine tendon has multiple $T_2$ components; (2) bovine nasal cartilage has a single $T_2$ component; and (3) canine articular cartilage has a single $T_2$ component. The $T_2$ profiles from both 5-point and 60-point methods were found to be consistent in articular cartilage. In addition, the depletion of the glycosaminoglycan component in cartilage by the trypsin digestion method was found to result in a 9.81% to 20.52% increase in $T_2$ relaxation in articular cartilage, depending upon the angle at which the tissue specimen was oriented in the magnetic field.

### Keywords

Multi-component; $T_2$; articular cartilage; bovine nasal cartilage; tendon; MRI; trypsin digestion; magic angle effect

## Introduction

The degradation of articular cartilage is a hallmark in musculoskeletal diseases such as osteoarthritis, which affects the majority of the senior population [1]. Due to the lack of specific and sensitive markers to detect subtle changes in the tissue, no routine procedure is currently available to assess nondestructively the functional, structural, and biochemical properties during the *early* stages of the tissue degradation. One major obstacle that has prevented any successful development of an early detection procedure is the complex molecular and morphological structures of the tissue. On the histological scale, the collagen fibrils (one of the three major molecules in cartilage) changes its spatial orientation significantly across the (thin) depth or thickness of the tissue [2]. (The other two major molecules are water and proteoglycans [3;4].) Consequently, articular cartilage is often regarded as consisting of three structural zones: the superficial zone (SZ) where the fibrils are parallel to the surface, the

*Corresponding Address: Yang Xia, Ph. D., Department of Physics, Oakland University Rochester, Michigan 48309, USA, Phone: (248) 370-3420, Fax: (248) 370-3408, Email: xia@oakland.edu.

transitional zone (TZ) where the fibrils are mostly randomly oriented, and the radial zone (RZ) where the fibrils are oriented perpendicularly to the surface [5;6;7;8;9]. This depth-dependent organization of the collagen fibrils in articular cartilage defines its depth-dependent anisotropy as viewed by many analytic and imaging instruments, such as the magic angle effect in MRI [8], birefringence in polarized light microscopy [2;10], and amide anisotropy in Fourier-transform infrared imaging [11;12;13].

Among the quantifiable parameters in MRI, $T_2$ relaxation is of particular importance since $T_2$ relaxation has been shown to be sensitive to the fibril structure/orientation and responsible for the MRI visualization of cartilage laminae (the so-called magic angle effect in MRI of cartilage [8]). In recent years, quantitative mapping of $T_2$ relaxation was able to detect the early structural changes in articular cartilage [14;15;16;17;18;19;20;21]. Furthermore, the anisotropy of $T_2$ relaxation has been used to divide the MRI-visible features of cartilage into MRI-zones nondestructively, which have been proved to be statistically equivalent to the histological zones based on the collagen orientation by quantitative polarized light microscopy [2;22;23].

In addition to the anisotropy of $T_2$ relaxation, the study of multi-components of $T_2$ relaxation [24;25] is also important in biological tissues such as the brain [26;27;28], nerve [29;30], muscle [31;32], tendon [33;34;35;36;37], and cartilage [35;38;39;40]. This is because these tissues are known to have several “pools” of water molecules, each with a distinct molecular environment [41;42]. Therefore, the ability to quantify the signal from each individual pool could enable the examination of sub-tissue populations and provide a better identification of early tissue degradation. Several studies have shown that the bulk $T_2$ in tendon and cartilage are multi-exponential. For example, Fullerton et al [33] considered the FID decays in bulk bovine tendons to be bi-exponential, with the short and long $T_2$ to be about 4 and 22 ms respectively. Peto et al [34] modeled the echo amplitudes from tendon with a four-component equation and found the four $T_2$ peaks at 0° orientation to be at 0.7, 4.7, 14.5, and 68 ms. These four $T_2$ components in tendon were confirmed by the $T_2$ distributions by Henkelman et al [35], who found four peaks at 2, 8, 23, and 56 ms. In bovine articular cartilage, Henkelman et al [35] demonstrated that the distribution of *bulk* $T_2$ relaxation had at least two peaks, centered around 20 and 55 ms at 0°, and that the 20ms peak largely disappeared when the tissue’s orientation was about 55° to the magnetic field.

The aim of this microscopic MRI (μMRI) project was to investigate if the multiple components of $T_2$ relaxation in articular cartilage could be resolved *in imaging* at high spatial resolution. In addition to canine articular cartilage (AC), bovine nasal cartilage (BNC) and canine tendon were also studied in this project. Unlike articular cartilage, tendon (bundles of collagen fibers to transfer the force experienced by muscle to the bone) does not have a zonal structure. The same is true in nasal cartilage. Consequently, for tendon and nasal cartilage, a low-resolution imaging or even a bulk experiment should produce the similar result as in high-resolution imaging. Two $T_2$ quantification methods were used in this μMRI project. In one method (5-point method), five $T_2$-weighted intensity images were acquired in μMRI, and a mono-exponential fitting was used to calculate a $T_2$ map at every pixel location in two dimensions. This is the most commonly used method in both clinics and laboratories (including our previous work), and is consistent with the fact that the fastest decay components in the tissue are not visible in MRI because of the long echo time. In the second method (60-point method), 60 $T_2$-weight intensity images were acquired for each specimen, which enables the calculation of multiple components of $T_2$ in the specimen. This method essentially results in a quantitative $T_2$ data cube, with two spatial dimensions and one dimension of $T_2$ distribution. We employed not only the conventional multivariable exponential fitting analysis but also the non-negative least-square (NNLS) method [24;43] [44] to analyze the $T_2$ distribution. Although this project was carried out using intact tissue blocks at microscopic resolution, it has direct relevance to

MRI of cartilage in general. It aimed to answer an important question: does a mono-exponential fitting of $T_2$ in MRI of cartilage result in an accurate $T_2$ value?

## Materials and Methods

Eight fresh specimens of articular cartilage were harvested from the central load-bearing area of three canine humeral heads. These dogs were skeletally mature and healthy, sacrificed for an unrelated experimental study. Each specimen consisted of the full thickness of the articular cartilage still attached to the underlying bone and had dimensions of about 1.75×2×10 mm. In addition to articular cartilage, three pieces of Achilles tendons were also harvested from the same canine origin and two pieces of bovine nasal cartilage were harvested from a local slaughter. All NMR/μMRI experiments were performed when the tissues were fresh, except as noted specifically. For imaging experiments, articular cartilage was soaked in physiological saline with 1% protease inhibitor (Sigma, Missouri). The experiments for tendon and BNC were carried out after the tissues were blotted dry.

NMR spectroscopic and microscopic MRI experiments were conducted at room temperature on a Bruker AVANCE II 300 NMR spectrometer equipped with a 7-Tesla/89-mm wide vertical-bore superconducting magnet and micro-imaging accessory (Bruker Instrument, Billerica, MA). A homemade 3mm solenoid coil was used for the cartilage-bone experiments, where the orientation of the collagen fibrils in the radial zone of the cartilage block with respect to the static magnetic field could be adjusted. Bovine nasal cartilage was also imaged using the same homemade coil. A Bruker 5mm birdcage coil with rotation device was used for the tendon experiments, where the long axis of the tendon sample was set at 55° (magic angle) relative to the direction of the magnetic field.

Spectroscopic measurements of bulk $T_2$ relaxation were performed using a standard CPMG pulse sequence,

$$90^\circ - (\tau - 180^\circ - \tau)_n - (acquisition). \quad (1)$$

A $\tau$ value of 500 μs was used in the experiments to avoid the spin-locking effect [45]. Only the even echoes were used in the experiments, where the last number of echoes was 800, which corresponds to an echo time of 800ms. The 90° rf excitation pulse had a duration of 8.38 μs and 3.69 μs for the nasal cartilage and tendon, respectively; the repetition time (TR) was 5 s; the number of dummy scans was 8.

Quantitative $T_2$ imaging experiments were performed using a magnetization-prepared CPMG $T_2$ imaging sequence (Fig 1), which is similar to the magnetization-prepared spin-echo $T_2$ imaging sequence that has been used extensively in our lab [46]. This sequence separates the leading $T_2$-weighting segment that contains no gradient pulse, and a subsequent imaging segment where all timings are kept constant, hence capable of giving an accurate measurement of $T_2$ in the tissue. The echo spacing in the CPMG $T_2$-weighting segment was 1ms, which was the same as that used in the spectroscopy experiments. Two sets of echo times had been used in the leading contrast segment for articular cartilage samples. In the first set (the 5-point method), the number of echoes were 2, 4, 10, 30, 60 for the articular cartilage when its surface was perpendicular to the static magnetic field and 2, 14, 36, 60, 120 when at the magic angle, respectively. In the second set (the 60-point method), the number of echoes had 60 increments; the last number of echoes was 710, which corresponds to an echo time of 710ms. For the first set (the 5-point method) experiment, the 2D imaging parameters were: echo time (TEi) was 8.6 ms; field of view (FOV) was 0.33 cm × 0.33 cm; imaging matrix size was 128 × 256 (256 was in the readout direction); the spectral bandwidth was 50 kHz corresponding to a 20 μs of

readout sampling dwell time; 1 ms and 0.75 ms sinc shape pulses were used as excitation and refocusing pulse in imaging segment, respectively. For the second set (the 60-point method) experiment, the following imaging parameters were used to minimize the echo time (TEi) and to achieve higher SNR: Field of view 0.33 cm × 0.33 cm; imaging matrix size 128 × 128; spectral bandwidth 100 kHz corresponding to a 10 μs of readout sampling dwell time; 0.8 ms and 0.507 ms hermite shape pulses were used as excitation and refocusing pulse, respectively. With these imaging parameters, an echo time of 3 ms in the imaging segment was achieved. The TR of the imaging experiment was 2 s. The in-plane pixel size, which was across the depth of the cartilage tissue, was 13 μm for the 5-point method and 26μm for the 60-point method. The 1mm-thick imaging slice was transversely located at the middle of the 10mm-long specimen. For tendon imaging experiments, all imaging parameters are the same except a larger FOV (1.2 cm × 1.2 cm) was used.

From the images acquired using the 5-point method, the $T_2$ relaxation in cartilage was calculated by a single exponential fitting of the data on a pixel-by-pixel basis, which assumes that there is only one $T_2$ component in cartilage. From the intensity images acquired using the 60-point method, the $T_2$ relaxation was calculated based on the same function by two methods, the nonnegative least-square (NNLS) method [24;43] implemented with the MatLab codes (MathWorks, Natick, MA) and the multi-variable exponential fitting in KaleidaGraph (Synergy Software, Reading, PA). The signal intensities as a function of the TEc (the echo time in the leading contrast segment) can be written as:

$$y(t_i)=\sum_{j=1}^{M} S_j e^{-t_i/T_{2j}}+C, \quad i=1,2,\ldots,\mathrm{N} \tag{2}$$

where $N$ is the number of echoes, $t_i$ is the $i^{th}$ TEc, $y(t_i)$ is the signal intensity of the $i^{th}$ echo, $M$ is the number of $T_2$ components, $S_j$ is the intensity of the $j^{th}$ $T_2$ component, and $C$ is a constant accounting for any offset of the signal. While we concentrated on the number of $T_2$ components, no additional constraint was incorporated into the least-squares misfit (Eq(7) in the reference [24]), which was minimized in NNLS algorithm. Therefore only a discrete spectrum of relaxation times was acquired from the data [24]. The bin spacing was 0.2 ms; the range of $T_2$ was from 0.2 ms to 400 ms ($M$ in Eq (2) was 2000). For each $T_2$ NNLS spectrum, the calculated $T_2$ components below a specific threshold (peak intensity less than 2% of the total intensity) were ignored to eliminate the dependence of the fit to the noise [27;32] [44]. All NNLS results in this report were also verified by the high R-values of the multi-exponential fitting method (in most cases, $R > 0.999$). The combination of the exponential fitting and NNLS method meant that the results in this report were acquired without *a priori* assumptions about the number of $T_2$ component and any initial guess of the solution.

Both 2D images and 1D profiles through the depth of the cartilage tissue in the 2D images were used for analysis and presentation. The 2D images enable us to examine any topographical variation in the images, whereas the 1D profiles enable us to examine the depth dependency of the results quantitatively and to compare the profiles from different imaging experiments. All images and profiles have consistent features among all specimens. Since there was no visible variation laterally within the tissue in these images, a rectangular region-of-interest (ROI) with a width of 10 contiguous columns were averaged from the 2D images to enhance the signal-to-noise ratio of the 1D profiles. The width and the location of the ROI were approximately the same in all specimens. There was no manual scaling or adjustment in plotting several cross-sectional profiles, which came from independent experiments, into one figure. Because the averaging occurs perpendicular to the tissue depth, the pixel resolution in the averaged profiles along the tissue depth is still 13μm and 26μm respectively.

# Results

## Proton Intensity Images

Canine tendon, bovine nasal cartilage and canine articular cartilage were studied using NMR spectroscopy and/or μMRI. Fig 2 shows the selected proton images from the representative $T_2$-imaging experiments where each μMRI experiment had 60 proton intensity images with different $T_2$ weightings. For the articular cartilage (Fig 2a and 2b), it is clear that the tissue has strong depth-dependent laminar structure when the tissue block is oriented with the normal axis of its surface parallel with the external magnetic field, which pointed upwards (Fig 2a, termed as the 0° orientation). This laminar appearance is due to the strong $T_2$ anisotropy in the superficial zone and radial zone of cartilage [47]. When the tissue block is oriented at the magic angle (Fig 2b, the 55° orientation), the minimization of the dipolar interaction results in higher $T_2$ relaxation in these two zones of cartilage, and hence brighter and more uniform images. For both bovine nasal cartilage (Fig 2c) and canine tendon (Fig 2d), there is no μMRI-visible structure in these intensity images.

## T2 Relaxation in Canine Tendon and Bovine Nasal Cartilage

The normalized signal from the NMR spectroscopy experiment of a canine tendon is shown in Fig 3a, where the decay of the signal is clearly not single-exponential. In addition to the long $T_2$ component of 362.5ms that was attributed to the residual free water on the surface of the specimen or NMR tube (see the insert), this set of spectroscopy data was analyzed by the NNLS algorithm to contain three $T_2$ components, shown in Fig 3b. With this *a priori* knowledge, multi-exponential fitting was also able to resolve three $T_2$ components from the signal, summarized in Table 1. The R-value of this fitting was 1, which means that the R value is larger than 0.999995 because only five significant figures are shown in KaleidaGraph. A visually convenient way of distinguishing whether the data is a single component or not is to plot the data in the natural log scale, shown in Fig 3c for both the spectroscopy and imaging results of canine tendon and in Fig 3d for the results of bovine nasal cartilage, respectively. Since tendon and nasal cartilage have no μMRI-visible structure in their intensity images, one averaged value was extracted from a 2D region-of-interest (10 pixels by 10 pixels) in the middle of each intensity image shown in Fig 2 to improve the signal-to-noise ratio (SNR). (The SNR of NMR spectroscopy and MR imaging (before the averaging) for the first data point were 31250 and 187 for tendon and 21250 and 380 for nasal cartilage respectively) It is clear that canine tendon has multiple $T_2$ components but bovine nasal cartilage has a single $T_2$ component.

## T2 Relaxation in Canine Articular Cartilage

The normalized proton signal from canine articular cartilage in the natural log format is shown in Fig 4a. Since articular cartilage has the depth-dependent morphological structure, every data point in Fig 4a comes from a 1D region-of-interest (1 pixel by 10 pixels) at a fixed tissue depth. The best SNR occurs where the tissue has the longest $T_2$ relaxation, i.e., in (1) all tissue locations when the tissue block is oriented at the magic angle and (2) the transitional zone when the tissue block is oriented at 0°. Within the limit of the imaging SNR (590, 685, 490 and 290 for the first data point at 26 μm, 104 μm, 234 μm and 364 μm location and after averaging) and given our voxel size ($26\mu m \times 26\mu m \times 1mm = 6.76\times10^{-4}$ $mm^3$), there is no visible multi $T_2$ component in articular cartilage. The NNLS algorithm was also used to verify this visual impression at every pixel along the entire tissue depth of cartilage imaging results; the results were consistently a single-component of $T_2$.

Fig 4b shows the depth-dependent $T_2$ profiles in fresh articular cartilage at 0° and 55°, where each point was calculated individually using the fitting method from all 60 data points from the imaging experiment after NNLS algorithm was performed first, the error bars are the fitting errors. These $T_2$ profiles agree well with the $T_2$ profiles from our previous cartilage imaging

work where only 4–5 data points were used [46]. It is clear that the errors in the fitting were extremely small. Fig 4c shows the histograms of the $T_2$ distribution in this fresh cartilage based on the interpolated $T_2$ profiles shown in Fig 4b, where the majority of the $T_2$ relaxation is centered around 54ms when the tissue is oriented at the magic angle and around 4ms when the tissue is oriented at 0°.

Several fresh articular cartilage blocks were treated biochemically using a 10mg/ml trypsin (Sigma-Aldrich, USA) digestion protocol [48], which removes the GAG macromolecules from the tissue. Data analysis of $T_2$ component identical to those used in Fig 4 were applied to this set of images, i.e., along the tissue depth from the articular surface to the bone at each pixel location. No multi-component $T_2$ was found within the limit of SNR at this voxel size. Fig 5a and 5b compare the calculated $T_2$ profiles for the fresh and trypsin-treated cartilage tissues at 0° and 55° respectively. The RMS averages of the entire T2 profiles in Fig 5a and 5b were 23.6 ±17.8ms for trypsin-treated tissue at 0°, 21.5±14.8ms for fresh tissue at 0°, 56.9±11.2ms for trypsin-treated tissue at 55°, and 47.2±8.7ms for fresh tissue at 55°. Several features can be identified. First, $T_2$ relaxation is sensitive to the GAG concentration in cartilage. After the depletion of GAG, the $T_2$ value increased, presumably due to the increased amount of water and the changed environment of water molecules in the tissue. Second, the sensitivity of $T_2$ to the GAG concentration maximized only when the influence of dipolar interaction was minimized; this happens at all tissue depths when the specimen is oriented at the magic angle (Fig 5b) as well as in the transitional zone when the specimen is oriented at 0° (Fig 5a).

Fig 5c shows the histograms of the $T_2$ distribution in this trypsin-digested cartilage based on the interpolated $T_2$ profiles shown in Fig 5a and 5b. Comparing with Fig 4c, it is clear that the enzymatic digestion shifted the $T_2$ distribution and the most obvious shift of the $T_2$ values occur when the specimen is oriented at 55°, toward higher $T_2$ values.

Several tissue blocks were also imaged using our ‘conventional 5-point’ $T_2$-imaging method, shown in Fig 6. Comparing with the $T_2$ images from 60-point method (Fig 5a and 5b), the 5-point method resulted in essentially the similar conclusion, i.e., $T_2$ was sensitive to the trypsin digestion, mostly sensitive when the specimen was oriented at the magic angles. This set of data also shows that the ‘detection sensitivity’, the $T_2$ difference between fresh and digested tissue, is less in the 5-point method. Fig 7 compares the $T_2$ profiles between the 5-image $T_2$ calculation and 60-image $T_2$ calculation. It is clear that both methods produce consistent results.

## Discussions

We have studied the multi-components of $T_2$ relaxation in cartilage and tendon using μMRI and NMR spectroscopy. Since articular cartilage is a thin layer of tissue with a complex depth-dependent structure, any quantification experiment for cartilage needs to be carried out at microscopic resolution, in order to minimize the volume averaging effect among the different molecular and structural environments in articular cartilage.

### Single vs. multi-component of T2 in tendon and cartilage

Within the limit of practical SNR in microscopic imaging, we have found in three different tissues that (1) tendon has multiple $T_2$ components; (2) nasal cartilage has single $T_2$ component; and (3) articular cartilage has single $T_2$ components in 26μm resolution along the depth of the tissue. Our tendon results are consistent with the NMR spectroscopy literature, where $T_2$ in tendon has been found to be multi-exponential [34;35]. Since tendon can be considered as a bundle of ‘uniformly oriented’ collagen fibers, the tendon result does not depend upon the resolution of the MRI/NMR experiments.

It should be point out that the ability to detect multi-components of $T_2$ in NMR/MRI can be influenced by several factors including the regularization algorithms and the inevitable experimental noises. For example, Moody and Xia found that a SNR threshold of about 300 was needed for detecting the presence of the sub-$t_0$ component with a probability of 0.9 or greater when using the second-derivative-squared regularizer in the linear regularization methods [44]. Although the SNR of cartilage ***imaging*** experiments in this report was not as good as we would like to have, it was probably better than any other imaging study of articular cartilage at this fine resolution. In fact, we have *purposefully* conducted an excessively long experiment to see if $T_2$ relaxation in articular cartilage could be measured to be multi-exponential, under these nearly impractical conditions. The answer was no.

The results of the single $T_2$ component in our articular cartilage experiments, however, would *appear* to be inconsistent with some literature results [35;38;40;49;50]. For example, Henkelman et al showed that articular cartilage had at least two $T_2$ components, centered around 20 and 55 ms when the tissue block was oriented at 0° [35]. This discrepancy in the number of $T_2$ components in articular cartilage comes from the fact that any full-thickness articular cartilage contains multiple molecular and structural architectures in its organization. If one does NMR spectroscopy or low-resolution MRI experiments, one averages among different architectures of the tissue, each having a unique characteristic. This can result in the observation of multiple $T_2$ components in bulk or large-voxel-imaging experiments. Another critical issue for reliable multi-component $T_2$ measurement is the need of sufficient data points to calculate $T_2$ [24;35]. In our μMRI experiments at high resolution, when the voxel size was reduced to $6.76\times10^{-4}$ $mm^3$ and 60 data points were acquired, we found that there was no multi-component $T_2$ in articular cartilage. This conclusion of a single component $T_2$ in articular cartilage is extremely beneficial to MRI $T_2$ mapping in general. Since there is only one $T_2$ component, one does not need to wonder whether a mono-exponential fitting of the high-resolution MRI signal is a faithful assessment of the true $T_2$ characteristics or not.

Our one $T_2$-component result in articular cartilage at all tissue depths, from the superficial zone to the deep zone, however, disagrees with the finding of Keinan-Adamsky et al [50], who showed that there were two $T_2$ components (5ms and 36–57ms) in a deep tissue (~ 20–60%) of porcine articular cartilage of 12 months or older. Since several key experimental details (eg, the thickness of imaging slice, the SNR, the shape and duration of the soft pulses used (which were important to understand the ultra short TE (2ms) used in that paper) were not disclosed in the Keinan-Adamsky report, one couldn't do a direct comparison between the Keinan-Adamsky experiment and our study. Comparing the actual $T_2$ values, one could wonder if it was possible that we have actually missed the *slow* (i.e., long) $T_2$ component in our experiments (the 36–57ms component in the Keinan-Adamsky report) in the deep zone (~ 20–60%)? The conclusion is no for the following three reasons. First, in our experiments, the $T_2$ value from the superficial zone to the radial zone changed continuously from 4 ms to about 60ms (by either NNLS or fitting method), which means that all $T_2$ values within this range could be detected in our experiments. Second, if the long $T_2$ component indeed existed in the deep tissue, the long $T_2$ component would be easier to detect than the short $T_2$ component, because the long $T_2$ component decays slower. Finally, the NNLS algorithm used in this report excluded *a priori* assumption about the number of exponentials.

Several models have been developed to explain the relaxation times and magnetization transfer in articular cartilage [40;46;51;52;53;54] and other biological system [55;56;57]. It is generally accepted that the proton dipolar interaction is the dominant relaxation mechanism in articular cartilage and that there are at least two proton pools in cartilage: free and bound water with chemical exchanges between them. When the chemical exchanges are faster than the relaxation processes, only one $T_2$ value can be measured in articular cartilage.

### The sensitivity of T2 on GAG concentration in articular cartilage

In most cartilage degradation cases in clinics, which portion of the tissue loss GAG *first* is probably unknown. It would also depend upon what is the trigger of the tissue degradation in each clinical case. For a majority of degradation that is initially diagnosed by a surface roughening, one can assume the GAG loss would be started at the first half of the tissue, which includes the transitional zone. This report demonstrates the depth-dependent 'sensitivity' of $T_2$ value towards the GAG depletion in articular cartilage. In the fresh vs. trypsin-treated $T_2$ profiles shown in Fig 5a and 5b, the changes in $T_2$'s RMS averages were 9.8% ((23.6 - 21.5)/ 21.5) when the specimen was oriented at 0° (Fig 5a) but increased to 20.6% ((56.9 – 47.2)/ 47.2) when the specimens was oriented at 55° (Fig 5b). This result shows that the sensitivity of $T_2$ relaxation to the GAG depletion in cartilage (one of the early signs of tissue degradation) can be doubled if the cartilage tissue is oriented towards the magic angle (~55°). Furthermore, if one has to measure the tissue degradation when the tissue cannot be oriented at 55° (most likely in human *in vivo* situations), one can still monitor the tissue regions around the transitional zone. Fig 5a shows that the $T_2$ value in transitional zone was still sensitive to the amount of GAG even though the tissue block was set at 0°, which has the strongest influence of the dipolar interaction.

On a related note, we showed in a previous work [48] that the cartilage GAG loss due to the trypsin incubation was time-dependent, reaching about 40% loss at 40 min of incubation, and about 70% GAG loss at 200 min incubation. Since the tissue blocks used in the previous work and this report are from the same origin (canine humeral cartilage blocks), and since the trypsin protocol in both studies are similar, we can assume that the GAG loss in the current project was also about 70%, which translates into approximately 20% $T_2$ increase in MRI.

Finally, the $T_2$ value itself from any biological experiment is a 'composite' measure of several rather complex factors, both at the molecular/structural levels in a biological specimen itself and at the procedural levels in the instrumentation/data-analysis. Consequently, it should be cautionary to attribute any small elevation or depletion in $T_2$ values to some interventional procedure. In this report, it might seem that $T_2$ in the deep part of the fresh cartilage at 0° were somewhat higher than the same in the trypsin-treated cartilage (200–500μm region in Fig 5a). A statistics comparison reveals such visual difference is actually very small: the RMS $T_2$ averages and standard deviations are 5.99±3.19 ms and 5.97±2.86ms for the fresh and trypsin-treated tissues respectively. However, the same experiments clearly confirm that the $T_2$ in the trypsin-treated specimen is significantly higher than the same in the fresh specimen (80–140μm region in Fig 5a). This distinct contrast between the deep tissue and the transitional zone tissue further demonstrates that the measurable $T_2$ difference ***in the transitional zone*** in this report was *not* due to any instrumentation/data-analysis factor, but due to the specimens themselves – one of the two had been trypsin-treated.

In conclusion, the experiments in this report investigated the multi-components of $T_2$ relaxation in three tissues: articular cartilage, nasal cartilage and tendon. While tendon has multi components of $T_2$, articular cartilage was found to have a single component of $T_2$ at microscopic resolution. This study provides an important message to the community of cartilage MRI: As long as one has sufficient resolution, a simple mono-exponential fitting of the $T_2$ data is a valid approach in the quantification of $T_2$ in cartilage. (When one has large voxels, as in clinical MRI, however, one can still have multiple $T_2$ components in MRI, simply because the co-existence of multiple environments.) In addition, the sensitivity of $T_2$ relaxation towards the GAG depletion was investigated. A strong influence of the specimen orientation in the magnetic field was found - One could double the 'detection sensitivity' if the specimen could be oriented towards the magic angle. Since a substantial improvement of image resolution in quantitative study of cartilage using the current MRI hardware and methodology is unlikely,

the microscopic results in this report can serve as the 'ultimate' characteristics of $T_2$ relaxation for future MRI study of articular cartilage.

## Acknowledgments

Y Xia is grateful to the National Institutes of Health for the R01 grants (AR 045172 and AR 052353). The authors are indebted to Dr. A Bidthanapally (Dept of Physics, Oakland University) for preparing the solutions used in this study, and Drs. C Les and H Sabbah (Henry Ford Hospital, Detroit) for providing the canine specimens. The authors thank Dr Kenneth P Whittall for his valuable insights in the use of NNLS calculation and Miss Carol Searight (Dept of Physics, Oakland University) for editorial comments.

## References

1. The Centers for Disease Control and Prevention, Press Release (October 24, 2002). (http://www.cdc.gov/od/oc/media/pressrel/r021024.htm)
2. Xia Y, Moody J, Burton-Wurster N, Lust G. Quantitative In Situ Correlation Between Microscopic MRI and Polarized Light Microscopy Studies of Articular Cartilage. Osteoarthritis Cartilage 2001;9:393–406. [PubMed: 11467887]
3. Maroudas A. Biophysical chemistry of cartilaginous tissues with special reference to solute and fluid transport. Biorheology 1975;12:233–248. [PubMed: 1106795]
4. Venn M, Maroudas A. Chemical composition and swelling of normal and osteoarthritic femoral head cartilage. Ann Rheum Dis 1977;36:121–129. [PubMed: 856064]
5. Clarke IC. Articular cartilage: A review and scanning electron microscope study. J Bone Joint Surgery 1971;53 B:732–750.
6. Bayliss M, Venn M, Maroudas A, Ali SY. Structure of proteoglycans from different layers of human articular cartialge. Biochem J 1983;209:387–400. [PubMed: 6405736]
7. Miosge N, Flachsbart K, Goetz W, Schultz W, Kresse H, Herken R. Light and electron microscopical immunohistochemical localization of the small proteoglycan core proteins decorin and biglycan in human knee joint cartilage. Histochem J 1994;26:939–45. [PubMed: 7896570]
8. Xia Y. Magic Angle Effect in MRI of Articular Cartilage - A Review. Invest Radiol 2000;35:602–621. [PubMed: 11041155]
9. Mow VC, Guo XE. Mechano-electrochemical properties of articular cartilage: their inhomogeneities and anisotropies. Ann Rev Biomed Eng 2002;4:175–209. [PubMed: 12117756]
10. Nieminen MT, Rieppo J, Toyras J, Hakumaki JM, Silvennoinen J, Hyttinen MM, Helminen HJ, Jurvelin JS. T2 relaxation reveals spatial collagen architecture in articular cartilage: a comparative quantitative MRI and polarized light microscopic study. Magn Reson Med 2001;46:487–93. [PubMed: 11550240]
11. Camacho NP, West P, Torzilli PA, Mendelsohn R. FTIR microscopic imaging of collagen and proteoglycan in bovine cartilage. Biopolymers 2001;62:1–8. [PubMed: 11135186]
12. Potter K, Kidder LH, Levin IW, Lewis EN, Spencer RG. Imaging of collagen and proteoglycan in cartilage sections using Fourier transform infrared spectral imaging. Arthritis Rheum 2001;44:846–55. [PubMed: 11315924]
13. Xia Y, Ramakrishnan N, Bidthanapally A. The depth-dependent anisotropy of articular cartilage by Fourier-transform infrared imaging (FTIRI). Osteoarthritis Cartilage 2007;15:780–788. [PubMed: 17317225]
14. Dardzinski BJ, Mosher TJ, Li S, Van Slyke MA, Smith MB. Spatial variation of T2 in human articular cartilage. Radiology 1997;205:546–50. [PubMed: 9356643]
15. Gründer W, Wagner M, Werner A. MR-microscopic visualization of anisotropic internal cartilage structures using the magic angle technique. Magn Reson Med 1998;39:376–82. [PubMed: 9498593]
16. Mosher TJ, Dardzinski BJ, Smith MB. Human Articular Cartilage: Influence of Aging and Early Symptomatic Degeneration on the Spatial Variation of T2 - Preliminary Findings at 3 T. Radiology 2000;214:259–266. [PubMed: 10644134]
17. Nieminen MT, Toyras J, Rieppo J, Hakumaki JM, Silvennoinen J, Helminen HJ, Jurvelin JS. Quantitative MR microscopy of enzymatically degraded articular cartilage. Magn Reson Med 2000;43:676–81. [PubMed: 10800032]

18. Olivier P, Loeuille D, Watrin A, Walter F, Etienne S, Netter P, Gillet P, Blum A. Structural evaluation of articular cartilage: potential contribution of magnetic resonance techniques used in clinical practice. Arthritis Rheum 2001;44:2285–95. [PubMed: 11665969]
19. Liess C, Lusse S, Karger N, Heller M, Gluer CC. Detection of changes in cartilage water content using MRI T2-mapping in vivo. Osteoarthritis Cartilage 2002;10:907–13. [PubMed: 12464550]
20. Gold GE. Dynamic and functional imaging of the musculoskeletal system. Semin Musculoskelet Radiol 2003;7:245–8. [PubMed: 14735424]
21. Alhadlaq H, Xia Y, Moody JB, Matyas J. Detecting Structural Changes in Early Experimental Osteoarthritis of Tibial Cartilage by Microscopic MRI and Polarized Light Microscopy. Ann Rheum Dis 2004;63:709–717. [PubMed: 15140779]
22. Xia Y, Moody J, Alhadlaq H, Burton-Wurster N, Lust G. Characteristics of Topographical Heterogeneity of Articular Cartilage over the Joint Surface of a Humeral Head. Osteoarthritis Cartilage 2002;10:370–380. [PubMed: 12027538]
23. Xia Y, Moody J, Alhadlaq H, Hu JN. Imaging the Physical and Morphological Properties of a Multi-Zone Young Articular Cartilage at Microscopic Resolution. J Magn Reson Imaging 2003;17:365–374. [PubMed: 12594728]
24. Whittall KP, MacKay AL. Quantitative interpretation of NMR relaxation data. J Magn Reson 1989;84:134–152.
25. Bronskill MJ, Santyr GE, Walters B, Henkelman RM. Analysis of discrete T2 components of NMR relaxation for aqueous solutions in hollow fiber capillaries. Magn Reson Med 1994;31:611–8. [PubMed: 8057813]
26. Gareau PJ, Rutt BK, Bowen CV, Karlik SJ, Mitchell JR. In vivo measurements of multi-component T2 relaxation behaviour in guinea pig brain. Magn Reson Imaging 1999;17:1319–25. [PubMed: 10576717]
27. Oh J, Han ET, Pelletier D, Nelson SJ. Measurement of in vivo multi-component T2 relaxation times for brain tissue using multi-slice T2 prep at 1.5 and 3 T. Magn Reson Imaging 2006;24:33–43. [PubMed: 16410176]
28. Qin Q, Gore JC, de Graaf RA, Does MD. Quantitative T2 measurement of a single voxel with arbitrary shape using pinwheel excitation and CPMG acquisition. Magma 2007;20:233–40. [PubMed: 17999101]
29. Does MD, Snyder RE. T2 relaxation of peripheral nerve measured in vivo. Magn Reson Imaging 1995;13:575–80. [PubMed: 7674853]
30. Stanisz GJ, Henkelman RM. Diffusional anisotropy of T2 components in bovine optic nerve. Magn Reson Med 1998;40:405–10. [PubMed: 9727943]
31. Prior BM, Foley JM, Jayaraman RC, Meyer RA. Pixel T2 distribution in functional magnetic resonance images of muscle. J Appl Physiol 1999;87:2107–14. [PubMed: 10601156]
32. Saab G, Thompson T, Marsh G. Multicomponent T2 relaxatoin of In Vivo Skeletal Muscle. Magn Reson Med 1999;42:150–157. [PubMed: 10398961]
33. Fullerton GD, Cameron IL, Ord VA. Orientation of tendons in the magnetic field and its effect on T2 relaxation times. Radiology 1985;155:433–435. [PubMed: 3983395]
34. Peto S, Gillis P. Fiber-to-field angle dependence of proton nuclear magnetic relaxation in collagen. Magn Reson Imaging 1990;8:705–12. [PubMed: 2266796]
35. Henkelman RM, Stanisz GJ, Kim JK, Bronskill MJ. Anisotropy of NMR properties of tissues. Magn Reson Med 1994;32:592–601. [PubMed: 7808260]
36. Gold GE, Pauly JM, Macovski A, Herfkens RJ. MR spectroscopic imaging of collagen: tendons and knee menisci. Magn Reson Med 1995;34:647–54. [PubMed: 8544684]
37. Takamiya H, Kusaka Y, Seo Y, Noguchi M, Ikoma K, Morimoto T, Hirasawa Y. Characteristics of proton nmr t(2) relaxation of water in the normal and regenerating tendon. Jpn J Physiol 2000;50:569–76. [PubMed: 11173552]
38. Lehner KB, Rechl HP, Gmeinwieser JK, Heuck AF, Lukas HP, Kohl HP. Structure, function, and degeneration of bovine hyaline cartilage: Assessment with MR imaging *in vitro*. Radiology 1989;170:495–499. [PubMed: 2911674]

39. Ghiassi-Nejad M, Torzilli PA, Peemoeller H, Pintar MM. Proton spin-spin relaxation study of molecular dynamics and proteoglycan hydration in articular cartilage [In Process Citation]. Biomaterials 2000;21:2089–95. [PubMed: 10966019]
40. Mlynarik V, Szomolanyi P, Toffanin R, Vittur F, Trattnig S. Transverse relaxation mechanisms in articular cartilage. J Magn Reson 2004;169:300–7. [PubMed: 15261626]
41. Maroudas, A. Different ways of expressing concentration of cartilage constituents with special reference to the tissue's organization and functional properties. In: Maroudas, A.; Kuettner, K., editors. Methods in Cartilage Research. Academic Press; London: 1990. p. 211-219.
42. Lancaster JL, Andrews T, Hardies LJ, Dodd S, Fox PT. Three-pool model of white matter. J Magn Reson Imaging 2003;17:1–10. [PubMed: 12500269]
43. Lawson, CJ.; Hanson, RJ. Solving Least Squares Problems. Prentice-Hall; Englewood Cliffs, New Jersey: 1974.
44. Moody JB, Xia Y. Analysis of multi-exponential relaxation data with very short components using linear regularization. J Magn Reson 2004;167:36–41. [PubMed: 14987596]
45. Santyr GE, Henkelman RM, Bronskill MJ. Variation in measured transverse relaxation in tissue resulting from spin locking with the CPMG sequence. J Magn Reson 1988;79:28–44.
46. Xia Y. Relaxation Anisotropy in Cartilage by NMR Microscopy ($\mu$MRI) at 14 $\mu$m Resolution. Magn Reson Med 1998;39:941–949. [PubMed: 9621918]
47. Xia Y, Farquhar T, Burton-Wurster N, Lust G. Origin of cartilage laminae in MRI. J Magn Reson Imaging 1997;7:887–894. [PubMed: 9307916]
48. Xia Y, Farquhar T, Burton-Wurster N, Vernier-Singer M, Lust G, Jelinski LW. Self-Diffusion Monitors Degraded Cartilage. Arch Biochem Biophys 1995;323:323–328. [PubMed: 7487094]
49. Mlynarik V, Degrassi A, Toffanin R, Vittur F, Cova M, Pozzi-Mucelli RS. Investigation of laminar appearance of articular cartilage by means of magnetic resonance microscopy. Magn Reson Imaging 1996;14:435–42. [PubMed: 8782182]
50. Keinan-Adamsky K, Shinar H, Navon G. Multinuclear NMR and MRI studies of the maturation of pig articular cartilage. Magn Reson Med 2006;55:532–40. [PubMed: 16450338]
51. Adler RS, Swanson SD, Yeung HN. A three-component model for magnetization transfer. Solution by projection-operator technique, and application to cartilage. J Magn Reson B 1996;110:1–8. [PubMed: 8556231]
52. Lüsse S, Knauss R, Werner A, Gründer W, Arnold K. Action of Compression and Cations on the Proton and Deuterium Relaxation in Cartilage. Magn Reson Med 1995;33:483–489. [PubMed: 7776878]
53. Lattanzio PJ, Marshall KW, Damyanovich AZ, Peemoeller H. Macromolecule and water magnetization exchange modeling in articular cartilage. Magn Reson Med 2000;44:840–51. [PubMed: 11108620]
54. Xia Y, Moody J, Alhadlaq H. Orientational dependence of T2 relaxation in articular cartilage: A microscopic MRI ($\mu$MRI) study. Magn Reson Med 2002;48:460–469. [PubMed: 12210910]
55. Fullerton G, Potter J, Dornbluth N. NMR relaxation of protons in tissues and other macromolecular water solutions. Magnetic resonance imaging 1982;1:209–228. [PubMed: 6927208]
56. Ling GN, Murphy RC. Studies on the physical state of water in living cells and model systems. II. NMR relaxation times of water protons in aqueous solutions of gelatin and oxygen-containing polymers which reduce the solvency of water for NA+, sugars, and free amino acids. Physiol Chem Phys Med NMR 1983;15:137–54. [PubMed: 6665043]
57. Watanabe T, Murase N, Staemmler M, Gersonde K. Multiexponential proton relaxation processes of compartmentalized water in gels. Magn Reson Med 1992;27:118–34. [PubMed: 1279356]

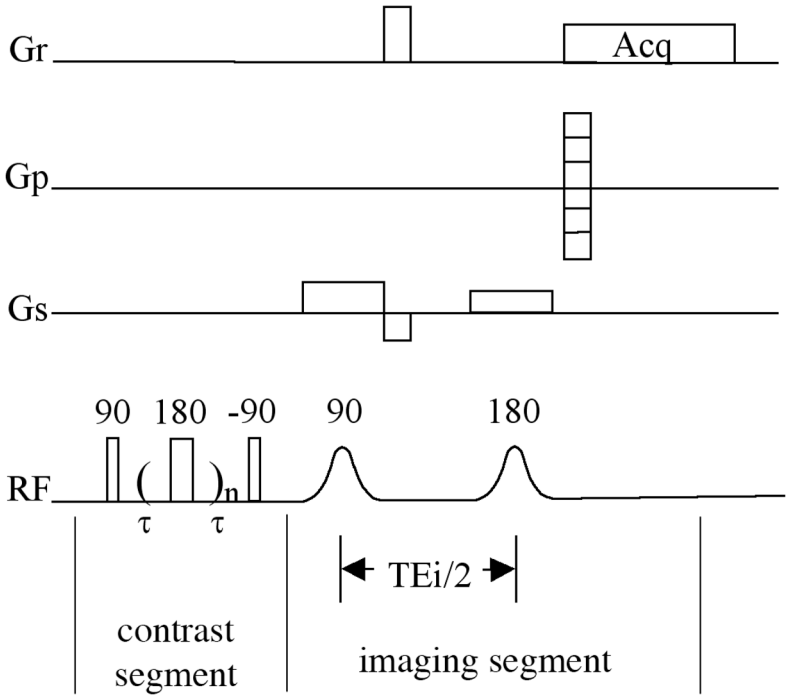


**Fig 1.**
The imaging pulse sequence that was used for the quantification of $T_2$ using CPMG.

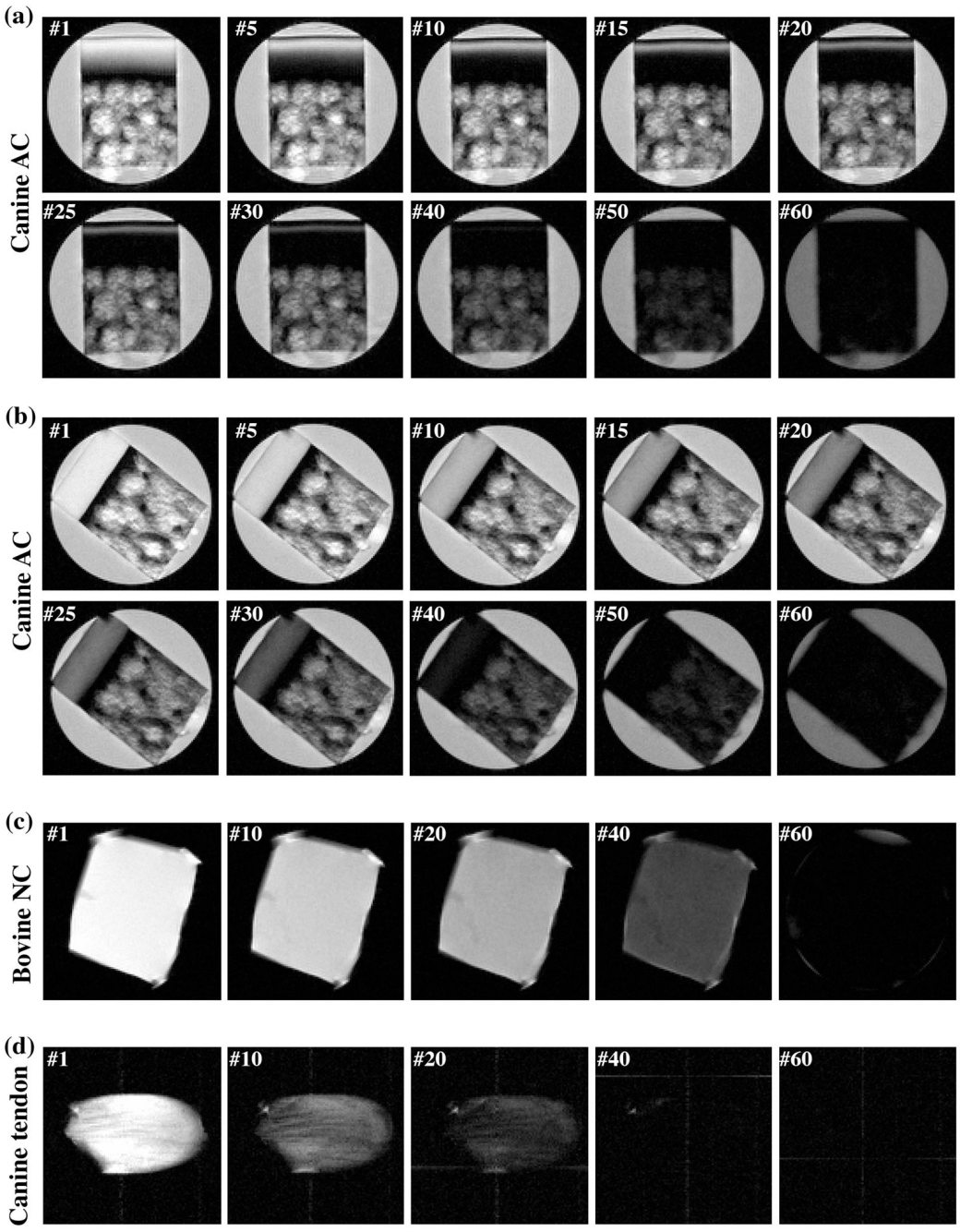


**Fig 2.**

Selected proton images from the μMRI experiments where each experiment had 60 proton images with different $T_2$ weightings, (a) a block of canine articular cartilage at 0° orientation, (b) a block of canine articular cartilage at the magic angle (55°), (c) a block of bovine nasal cartilage, and (d) a block of canine tendon. All images were displayed using the same minimum and maximum values. (AC: articular cartilage; NC: nasal cartilage)

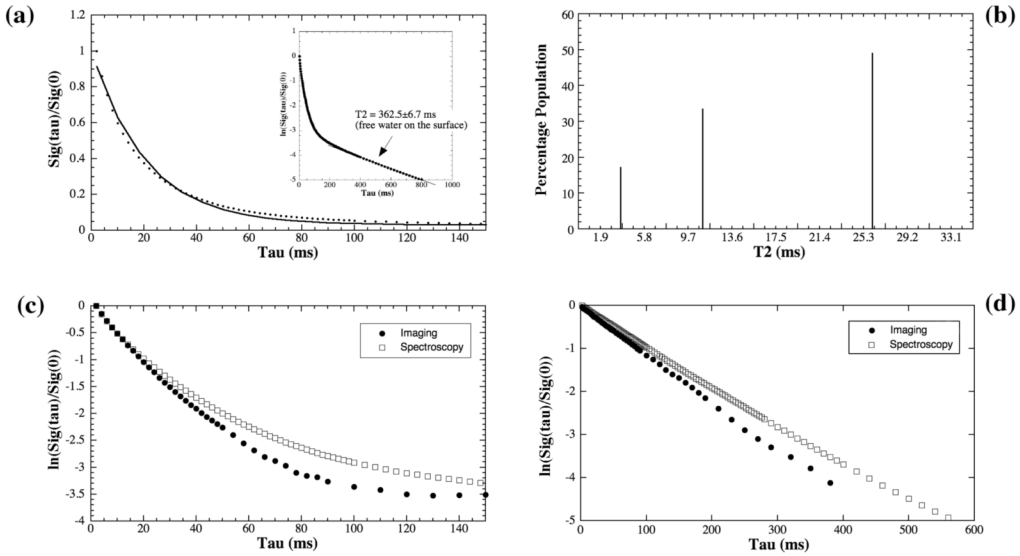


**Fig 3.**

(a) The normalized signal decay in the NMR spectroscopy experiment of a canine tendon, where the solid line in the main figure is an exponential fit with one decay-constant (i.e., one $T_2$ component). (b) The NNLS results using the same data in (a), where three $T_2$ components were found. (c) The natural log plot of the canine tendon data from both NMR spectroscopy and μMRI, where the curvatures of the log plot show visually the multi $T_2$ component of the specimens. (d) The natural log plot of the bovine nasal cartilage data from both NMR spectroscopy and μMRI, where the linearity of the log plot show visually single $T_2$ component of the specimens.

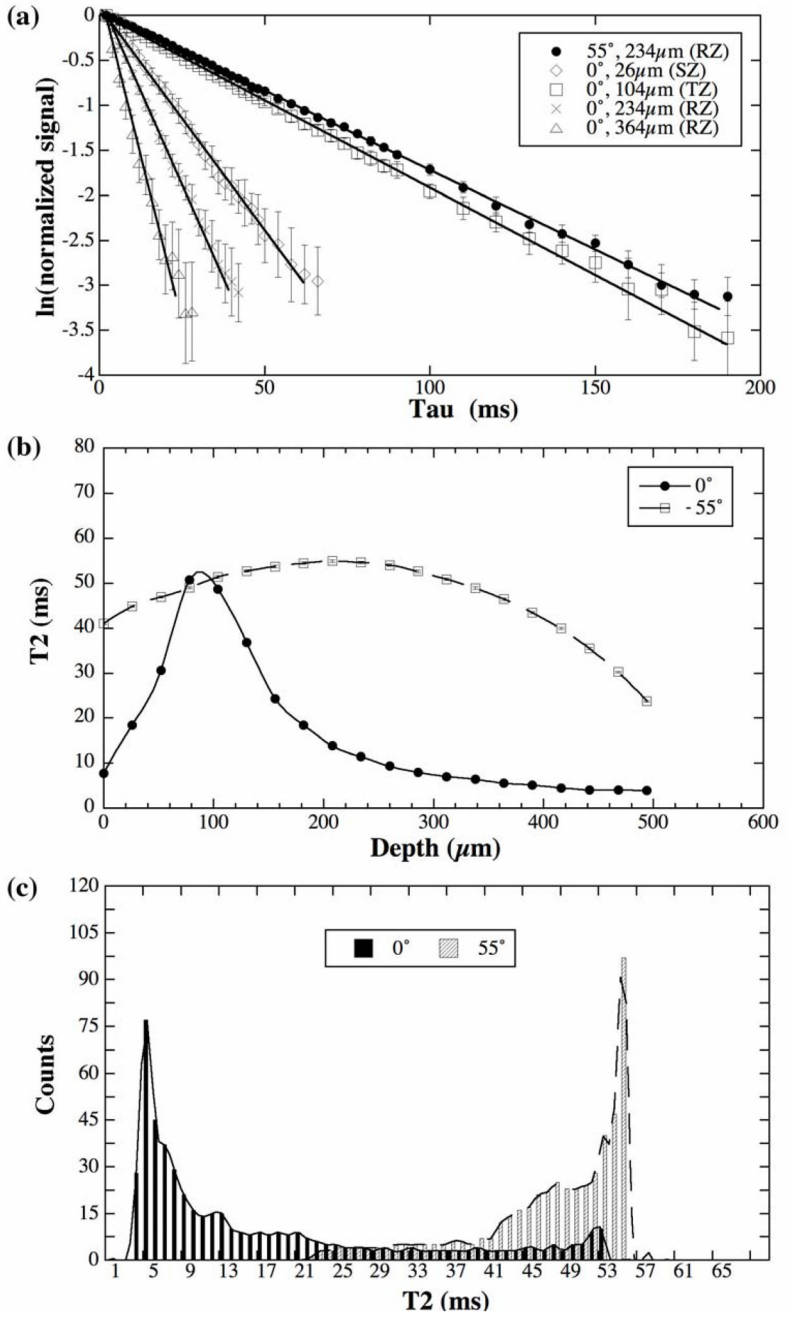


**Fig 4.**

Fresh canine articular cartilage data from the 60-image μMRI experiments. (a) The natural log plots of the μMRI data of healthy canine articular cartilage, where each plot was from a single pixel location at different zones in articular cartilage. (b) The depth dependent $T_2$ profiles in healthy articular cartilage at 0° and 55°, where each point was calculated individually using the NNLS algorithm. (c) The histograms of the $T_2$ distribution in healthy cartilage based on the interpolated T2 profiles shown in (b). (Note that some error bars, which have been plotted in (a) and (b), are within the symbols.)

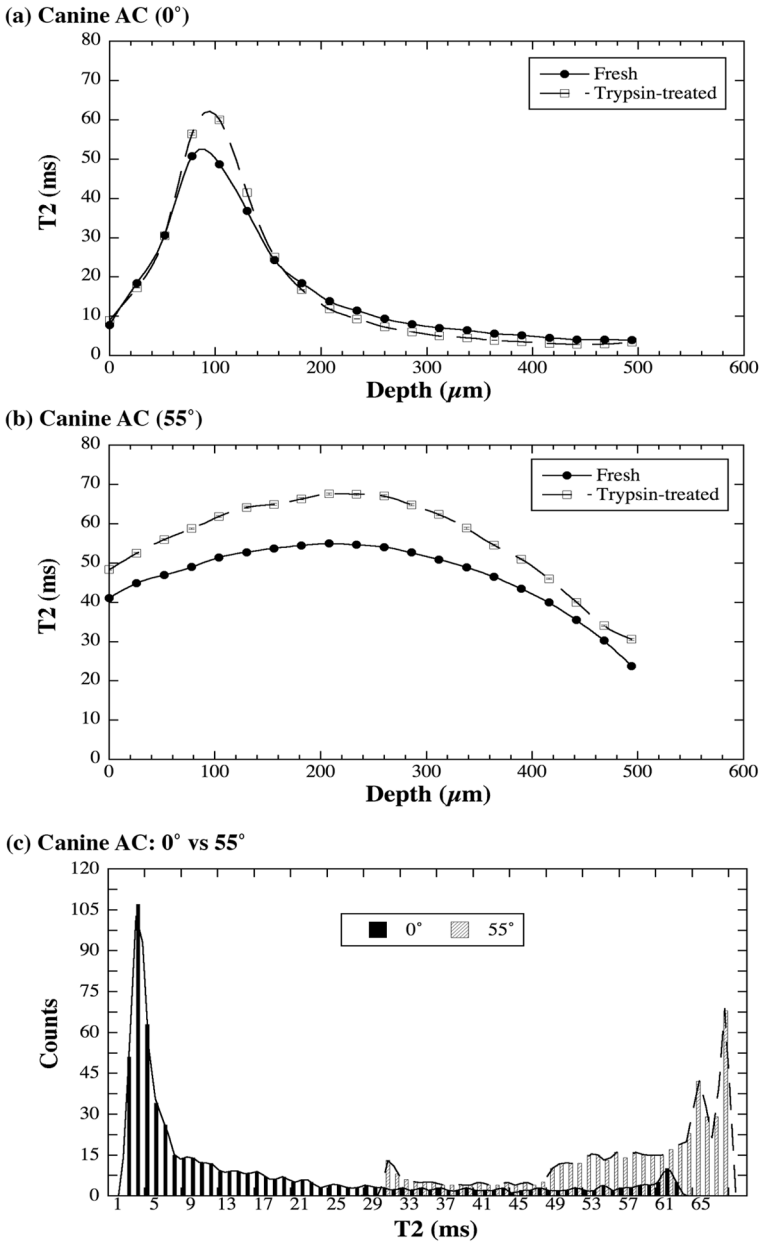


**Fig 5.**

Trypsin-treated canine articular cartilage data from the 60-image μMRI experiments. The comparisons between the $T_2$ profiles of fresh and trypsin-treated cartilage were shown in (a) and (b). (c) The histograms of the $T_2$ distribution in trypsin-treated cartilage based on their interpolated $T_2$ profiles, which show the increased $T_2$ values in the GAG-depleted cartilage. (The error bars have been plotted in (a) and (b).)

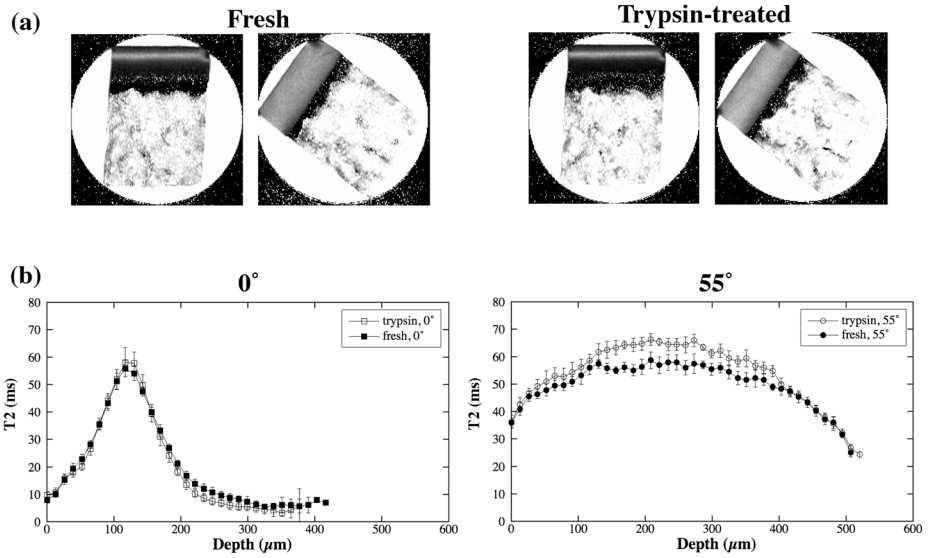


**Fig 6.**

Canine articular cartilage data from the 5-image μMRI experiments. The $T_2$ images (a) and profiles (b) of fresh and trypsin-treated articular cartilage.

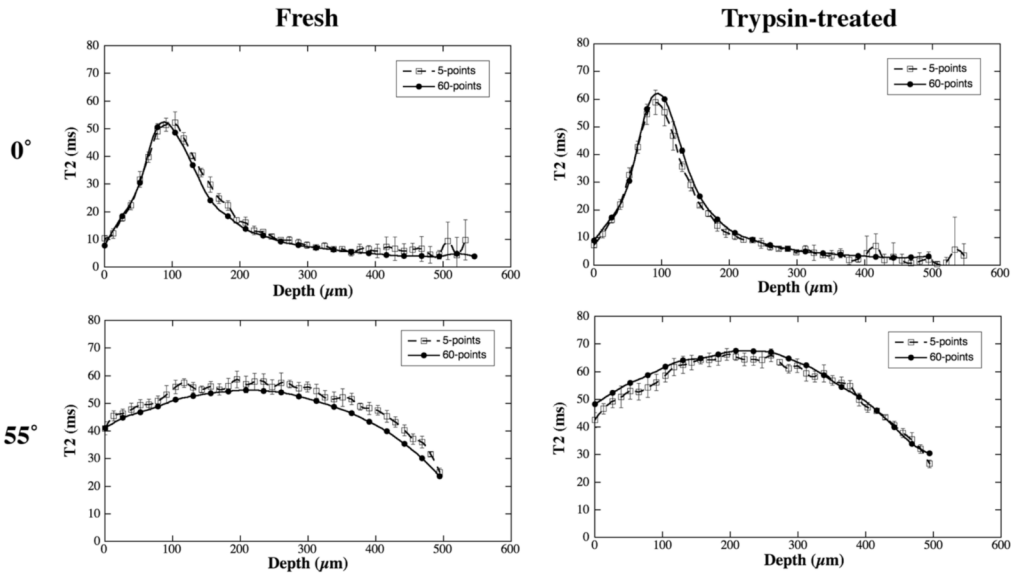


**Fig 7.**
Comparison for the $T_2$ profiles between the 5-image $T_2$ calculation and 60-image $T_2$ calculation in μMRI.

**Table 1**

Comparison of multi-component T2 in Tendon and Bovine Nasal Cartilage (BNC)

| | Bulk from Spectroscopy | | | | Bulk from Imaging | | | |
|---|---|---|---|---|---|---|---|---|
| | Exp Fit (KG) | | NNLS (MatLab) | | Exp Fit (KG) | | NNLS (Matlab) | |
| | T2 (ms) | % | T2 (ms) | % | T2 (ms) | % | T2 (ms) | % |
| tendon | 3.6±0.1 | 30.8 | 3.7±0.2 | 17.3 | 1.7±0.9 | 7.5 | 1.6±0.9 | 7.5 |
| | 12.5±0.2 | 29.1 | 11.0±0.4 | 33.6 | 8.1±1.0 | 26.9 | 8.0±0.3 | 26.4 |
| | 29.1±0.2 | 40.1 | 26.1±0.6 | 49.1 | 21.0±0.4 | 65.6 | 20.9±0.8 | 66.1 |
| BNC | 98.9±0.9 | 100 | 96.0±0.9 | ~100* | 88.3±0.5 | 100 | 85.5±0.9 | ~100* |

*There were some minor deviations (~ 2%) in bovine nasal cartilage; but we concluded that they were caused by the noises in the data.